BIOCHEMISTRY
including biophysical chemistry & molecular biology
Article

Biochemistry **2009,** *48,* 9061–9075 9061
DOI: 10.1021/bi900585m

Catalytic Mechanism of DNA Backbone Cleavage by the Restriction Enzyme EcoRV: A Quantum Mechanical/Molecular Mechanical Analysis†

Petra Imhof,‡ Stefan Fischer,*,§ and Jeremy C. Smith‡,∥

‡*Computational Molecular Biophysics, IWR, University of Heidelberg, Im Neuenheimer Feld 368, 69120 Heidelberg, Germany,* §*Computational Biochemistry, IWR, University of Heidelberg, Im Neuenheimer Feld 368, 69120 Heidelberg, Germany, and* ∥*Oak Ridge National Laboratory, P.O. Box 2008 MS 6309, Oak Ridge, Tennessee 37831-6309*

Received April 6, 2009; Revised Manuscript Received August 11, 2009

ABSTRACT: Endonucleases, such as the restriction enzyme EcoRV, cleave the DNA backbone at a specific recognition sequence. We have investigated the catalytic mechanism of backbone phosphodiester hydrolysis by the restriction enzyme EcoRV by means of hybrid quantum mechanical/molecular mechanical calculations. An exhaustive computation of different reaction pathways is performed, thus generating a network of pathways. Comparison of the computed (AM1d/MM) enzymatic reaction pathways with an analogous mechanism for small-molecule model systems [AM1/d and B3LYP/6-31++G(d,p)] reveals that the transition barriers for associative hydrolysis, which is more probable in the model systems, are not lowered by the enzyme. Instead, a reaction mechanism which has mostly dissociative character is more likely. The protein environment is tuned to significantly electrostatically stabilize the transition state structures. The direct catalytic impact of essential residues is determined: The magnesium metal ion activates a water molecule, thus facilitating protonation of the leaving group. A reduction of the coordination number of the magnesium metal ion from six to four upon the positioning of the attacking water molecule explains why larger metal ions, such as calcium, are not catalytically active. The nucleophile is generated by the transfer of a proton from the attacking water molecule to a carboxylic oxygen atom of aspartate 90. The catalytic effect of lysine 92 involves proper positioning of the scissile phosphate group and, more importantly, stabilization of the metaphosphate intermediate in an orientation optimal for attack of the nucleophile.

EcoRV is a type II restriction enzyme from *Escherichia coli* that recognizes and cleaves the DNA sequence GAT↓ATC [where ↓ marks the cleavage site (*1*)]. Endonucleases accelerate the hydrolysis of phosphodiester bonds by a factor of at least 10^{15}, compared to the uncatalyzed reaction in aqueous solution (*2*−*4*). Understanding how these enzymes function is of fundamental biological and chemical interest.

There is considerable literature on crystallographic data available for this enzyme (*5*−*15*), as well as on mutagenesis work (*8*, *16*) and kinetic studies (*17*−*21*). On the basis of these data, the identity of the catalytically essential residues has been identified. However, their precise role and the detailed reaction mechanism of EcoRV have not been determined.

The amino acids Asp90, Asp74, and Lys92 have been identified as the most important catalytic residues in EcoRV. These three amino acids are the only active site groups conserved among a subset of type II restriction endonucleases which possess the signature sequence PD...(D/E)XK and in which the positions of the side chain groups and scissile phosphates are superimposable with each other and with those of EcoRV (*22*). Furthermore, their structural proximity to the scissile phosphate groups is consistent with these residues being important for catalysis. In addition, the side chains of Asp90 and Asp74 are both ligands to a divalent metal ion which forms a bridge to the scissile phosphate (*12*, *23*, *24*). In some crystal structures, Asp74 also chelates a second divalent metal ion. Upon mutation of Asp90 or Asp74 to alanine, no catalytic activity is observed, and upon mutation of Lys92 to alanine, the catalytic activity of EcoRV is approximately 10^5-fold reduced (*6*, *8*, *25*). The primary role of Asp90 and Asp74 is believed to be the binding of divalent metals, but the function of Lys92 is less clear. Transition state stabilization seems to be unlikely due to the position of the Lys92 amine on the same side of the scissile phosphate as that on which the new P−O bond is formed (*9*, *12*, *26*). Depending on its protonation state, Lys92 may help stabilize and orient a hydroxide ion for nucleophilic attack (if positively charged) or function as a catalytic base to accept a proton from the attacking water (if neutral) (*8*, *26*). The latter possibility is supported by the finding that the reaction chemistry proceeds optimally at a relatively high pH of 8.5 (*14*).

In addition to the key amino acid residues mentioned above, the presence of divalent cations is essential for the function of restriction enzymes (*4*, *5*, *14*, *17*). The native metal ion is magnesium, although it can be replaced in vitro by, for example, a manganese or zinc ion. With calcium as the metal cofactor, complex formation has been observed but not hydrolysis (*27*−*29*). The role of the metal ion(s) is still a matter of debate as is the required number of divalent metal ions per subunit. One role ascribed to the metal cofactor is stabilization of the double negatively charged transition state (*9*, *12*). Another possible role is nucleophile activation: the association with a Mg^{2+} ion lowers

†Supported by the DFG as part of the SFB623 "Molecular Catalysis", the University of Heidelberg with a Olympia-Morata fellowship (P.I.), and a Laboratory-Directed Research and Development grant from the U.S. Department of Energy (J.C.S.).

*To whom correspondence should be addressed. E-mail: stefan.fischer@iwr.uni-heidelberg.de. Phone: ++49-6221-548879. Fax: ++49-6221-548868.

Published on Web 08/13/2009

the pK_a value of a water molecule and thus facilitates generation of a hydroxide ion which is the better nucleophile. A third possible role is activation of an inner-sphere-bound water molecule, hydrogen bonded to the 3′-oxygen, that serves as a proton donor to the leaving group (*14*). Metal ions might also enhance the reaction by placing the nucleophile in a position favorable for attack at the phosphorus atom.

From several crystal structures, there is a consensus about the position of the first metal binding site, which is located at the scissile phosphate group and ligated by the carboxylic groups of residues Asp74 and Asp90 (*12*, *23*, *24*). A second binding site is formed by the carboxylic groups of residues Asp74 and Glu45. Reference *30* reports a third metal ion site for a T93A mutant, bound to DNA and Ca^{2+}: the divalent metal ion in this site bridges via a water molecule to one oxygen of the 3′-adjacent phosphate and ligates a second water molecule which is located approximately in-line for attack on the scissile phosphate. However, the experimental data suggest that all three binding sites are never occupied at the same time (*30*).

The stereochemical course of the phosphate transfer reaction has been investigated for a number of nuclease enzymes (*31*). These enzymes can be divided into two classes: those which react with inversion of configuration at the scissile phosphorus and those which show retention. Most phosphodiester cleavage reactions have been reported to occur with inversion (*32*). Reference *19* reports that the DNA cleavage reaction conducted in $H_2{}^{18}O$ by the restriction enzyme EcoRI proceeds with inversion of configuration, thus excluding a covalent enzyme−substrate intermediate, which would require two such substitution reactions with inversion resulting in a net retention of configuration. Whether the cleavage reaction follows an associative or dissociative mechanism remains an open question. Free in solution, a fully dissociative mechanism (like SN1 in carbon chemistry) would lead to racemization. However, within an enzyme active site, steric crowding and the departing leaving group may prevent nucleophilic attack from the side on which the leaving group is located. An associative (SN2) mechanism via a bipyramidal intermediate or transition state would clearly lead to inversion of configuration. In principle, any variant between fully associative and fully dissociative is conceivable, and all would be consistent with inverted phosphorus products in an enzymatic environment.

In this work, we report on a computational study with hybrid quantum mechanical/molecular mechanical (QM/MM)[1] methods to model the hydrolytic DNA cleavage catalyzed by the restriction enzyme EcoRV with the aim of elucidating the detailed reaction mechanism and identifying key residues and their precise roles in the course of the reaction.

This paper is organized as follows. A Methods section describes the setup and the computational details for active site model calculations, the generation of the enzymatic reactant and product state models, and the QM/MM pathway calculations. The Results section presents the findings of the reaction pathway calculations for active site models and the enzymatic mechanism, which are then discussed and compared to the experimental findings known from the literature. The paper concludes with a summary of the key points.

[1]Abbreviations: AM1, Austin Model 1; B3LYP, Becke's three-parameter density functional; DFT, density functional theory; QM/MM, quantum mechanical/molecular mechanical; CPR, conjugate peak refinement; NUCS, nonuniform charge scaling; PDB, Protein Data Bank; RC, reaction coordinate.

METHODS

1. Small-Molecule Model Systems. We have examined models for the enzymatic phosphodiester cleavage at two different levels of theory. (1) Density functional theory (DFT), applying Becke's three-parameter hybrid functional B3LYP with a 6-31++G(d,p) basis set was used. The DFT calculations were performed with the Turbomole program package (*33*). (2) The same pathways were computed applying AM1/d (AM1 with extension to d-orbitals for the elements magnesium and phosphorus), which was also used for the hybrid QM/MM computation of the enzymatic pathways as described below.The AM1/d parameters for magnesium were taken from ref *34*, and the phosphorus parameters are based on those published in ref *35*, refined for the reaction under study in this work. The phosphorus parameters are listed in the Supporting Information. For oxygen and hydrogen, the parameters used were published in ref *36*. For the AM1/d calculations, the MNDO96 program package (*37*) was used. An evaluation of the performance of the AM1/d method compared to a B3LYP/6-31++G(d,p) reference for proton affinities of magnesium-bound Asp (modeled as acetate) and monodentate versus bidentate Mg^{2+} ligation by Asp is represented as Supporting Information. For this, we have compared reaction energies calculated at the two levels of theory. Proton affinities have been computed as the reaction energies for transfer of a proton from a water molecule to the Asp residue, resulting in a protonated Asp and a hydroxide ion.

Geometries of stationary points were optimized to a gradient of 10^{-4} E_h/Bohr. The conjugate peak refinement (CPR) algorithm (*38*) as implemented in CHARMM (*39*) was used to determine transition states between the pairs of given end states of the elementary steps of the reactions. The criterion for accepting a saddle point was an initial gradient of 10^{-2} kcal mol^{-1} Å^{-1} to be satisfied for six line-minimizations in the CPR. The nature of the stationary point (minimum or transition state) was subsequently verified by normal-mode analysis on the optimized geometries.

In addition to the vacuum calculations, the hydrolysis pathways were computed at the DFT level of theory in implicit solvent (dielectric constant $\varepsilon = 80$), making use of the conductor-like screening model (COSMO) (*40*). The criterion for geometry convergence was set to 10^{-3} E_h/Bohr. Calculation of numerical second derivatives served to identify minima and saddle points.

2. Enzyme Model System. The enzyme model system is based on three X-ray structures (*23*, *30*). One of these is a mutant in which Lys92 is mutated to alanine (PDB entry 1SX8). The back mutation to the wild type was modeled starting from the coordinates of this residue from a closely related structure (PDB entry 1RVB) (*23*). Metal ions (initial positions taken from PDB entry 1SUZ), and crystallographic water molecules were added as also determined crystallographically. Hydrogen atoms were added using stereochemical criteria. Thirty-six crystallographic water molecules were also included. The complex was hydrated in an octahedral water box with 13347 water molecules (leading to a total of 48825 atoms), and octahedral periodic boundary conditions were applied. Energy minimization was performed to a gradient of 0.01 kcal mol^{-1} Å^{-1}. Molecular dynamics (MD) heating and equilibration were performed with velocity scaling for 20 and 300 ps, respectively. The MD production phase was 1 ns at 1 bar and 300 K applying a Nosé-Hoover barostat and thermostat (*41*, *42*). Bonds containing hydrogen atoms were

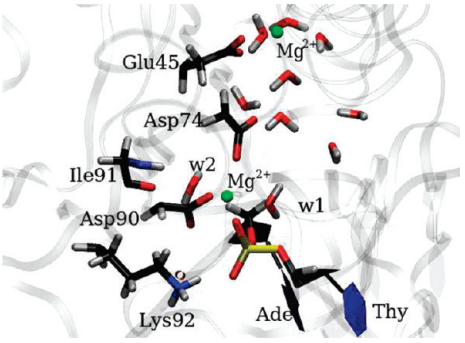

FIGURE 1: Optimized reactant state. Quantum mechanically treated atoms are shown explicitly, and the remainder of the protein (ribbon representation) is represented with molecular mechanics.

constrained (*43*) permitting extension of the integration time to 2 fs. The MD simulations were conducted using CHARMM (*39*).

A snapshot from the molecular dynamics ensemble, taken to possess average values for some important geometric parameters (see Enzymatic Reactant Complex in Results section) served as the initial structure for further optimization of the reactant state (QM/MM Setup) and subsequent modeling of the reaction pathways.

In this work, we model the DNA cleavage reaction in one subunit only. Simultaneous modeling of the hydrolysis in the two subunits with two distinct quantum mechanically treated regions in a hybrid QM/MM setup is not feasible. This approach prevents the direct use of the available crystal structures of the product complex with the DNA cleaved in the two subunits. Instead, we modeled a complex with cleaved DNA in only one subunit by setting the positions of the active site atoms to those from the product complex crystal structures with PDB entry 1SX5 from ref *30*, aligned with the equilibrated reactant complex which was modeled as described above. All other atoms were assigned to the same initial positions as in the reactant state. This approach is justified by the outer part of the protein differing negligibly between the reactant and product state complex crystal structures. The subsequent geometry optimization was performed with the QM/MM setup described below.

3. QM/MM Setup. All energy minimization and pathway calculations in the enzyme were performed with a combined QM/MM setup. The quantum mechanical region comprises dimethyl phosphate to mimic the DNA backbone, two magnesium ions, the side chains of amino acids Asp90, Asp74, Glu45, and Lys92, the backbone atoms of amino acid Ile91, and the water molecules located in the active site of one subunit (cf. Figure 1).

The QM/MM boundary was treated with the link atom approach (*44*). For the quantum mechanical calculations, we used the semiempirical method AM1/d, and the molecular mechanical part was modeled with the CHARMM force field (*39*).

To keep the number of degrees of freedom for the hydrolysis reaction minimal, only those water molecules located in the active site (12 per subunit) were treated explicitly. For the representation of the solvent and the other buried water molecules, we applied the nonuniform charge scaling (NUCS) procedure as described in ref *45*, in which the charges of the molecular mechanically treated atoms are scaled in such a way that the interaction energies of groups of atoms, calculated in vacuo (with these scaled charges), best match the interaction energy values calculated with a Poisson−Boltzmann implicit solvent treatment.

Comparison of the available crystal structures of EcoRV−DNA complexes with intact and cleaved DNA indicates that the outer part of the protein does not undergo significant conformational changes during the hydrolysis reaction. Thus, the number of degrees of freedom was further reduced by fixing all atoms more than 10 Å from the Mg ions to their positions in the reactant state.

All QM/MM calculations were carried out with CHARMM version c28b1 (*39*) interfaced to the MNDO96 program (*37*).

4. Reaction Pathway Calculations. A large number of potential reaction pathways were computed and are schematically depicted in Figure 2. The pathways consist of the following elementary steps: generation of the nucleophile (a hydroxide ion), nucleophilic attack, protonation, and departure of the leaving group. The pathways consist of a subset of possible transitions, focusing on those residues which are closest to the scissile phosphate group and as such are likely to have the largest impact on catalysis. Note that the active site region treated quantum mechanically is larger than the subset of residues shown in Figure 2 and includes additionally the second magnesium ion, the side chain of Glu45, the backbone of Ile91, and more water molecules. The subset of transitions investigated involves only those which are likely to be productive, so for example, proton transfers to distant atoms were not studied.

Two types of reaction pathways can be distinguished: (1) dissociative pathways, in which the P−O bond is cleaved and the leaving group departs before the nucleophile attacks, and (2) associative pathways, which exhibit nucleophilic attack prior to dissociation of the scissile phosphodiester bond. Possible intermediates of the dissociative pathway are denoted with "d" in Figure 2, and those of the associative pathway are labeled with "a".

The nucleophile in all of the pathways sketched in Figure 2 is the deprotonated water molecule, w2. The nucleophile is generated by transfer of a proton to either a carboxylic oxygen atom of the side chain Asp90 or one of the oxygen atoms of the scissile phosphate group (O1 or O2). The proton transfer to O2 can be mediated by the nearby side chain of Lys92 (step Ra1 or step d1d2). The leaving group can be protonated by either water molecule w1 (step Rd1 or a2d2) or transfer of the proton placed at O1, O2, or Asp90 after nucleophile generation (step a2P). In the scenario with w1 as the proton donor, reprotonation can again occur by transfer of a proton from O1, O2, or Asp90 (step d2P).

P−O bond breaking and formation and the proton transfer steps are accompanied by conformational rearrangements, such as side chain reorientation, and the movement of water molecules, including, most importantly, the repositioning of the attacking water molecule.

Intermediate states were generated by placing protons and changing P−O distances. The geometries of the reactant, product, and intermediate states were optimized to a gradient of 10^{-4} kcal mol^{-1} Å^{-1}. Reaction pathways and the associated transition states were determined using the conjugate peak refinement (*38*) algorithm as implemented in CHARMM (*39*). The criterion for accepting a saddle point was an initial gradient of 10^{-2} kcal mol^{-1} Å^{-1} to be satisfied for 33 line-minimizations in the conjugate peak refinement.

RESULTS

1. Small-Molecule Model Systems. As a small-molecule model for DNA backbone hydrolysis, we computed a dissociative and an associative reaction pathway for the hydrolysis of pentaquo-magnesium-dimethylphosphate. The stationary points

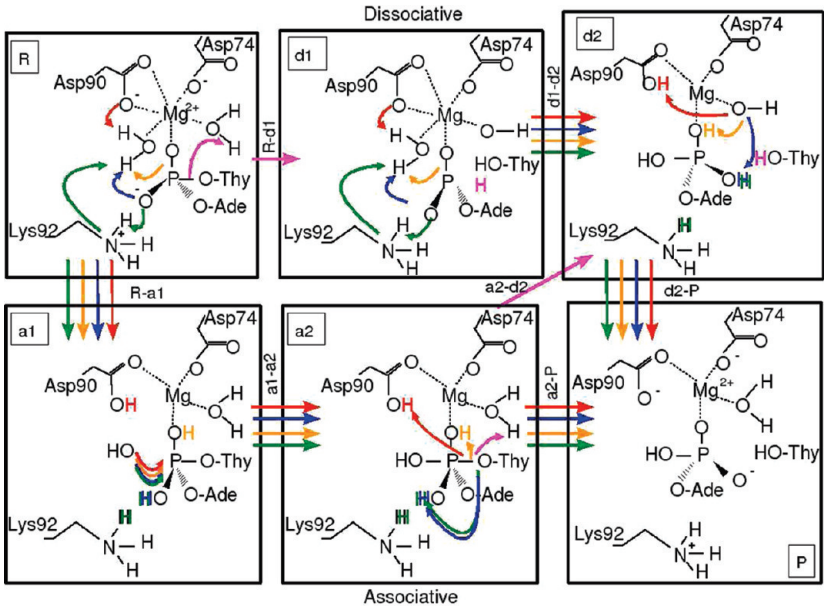

FIGURE 2: Scheme of pathways investigated for DNA hydrolysis by EcoRV. For the sake of clarity, charges are shown only for reactant and product states. Intermediate states for dissociative pathways (top route) are labeled d1 and d2. Those for associative pathways (bottom route) are labeled a1 and a2. R and P denote reactant and product states, respectively. Curved arrows indicate the movement of atoms in the transition to the next state. Different pathways are distinguished by colors. Straight arrows point to the final state of the respective transition. The colored atoms mark the different possible positions according to the different possible transitions. For example, the red-colored hydrogen atom in state a1 results from the transfer of a proton from water molecule w2 to Asp90, represented as a red arrow in the subfigure of state R. The transition from state a1 to state a2 involves the same movement for all possibilities (i.e., the hydrogen atom located at the different colored positions), i.e., attack of the hydroxide ion.

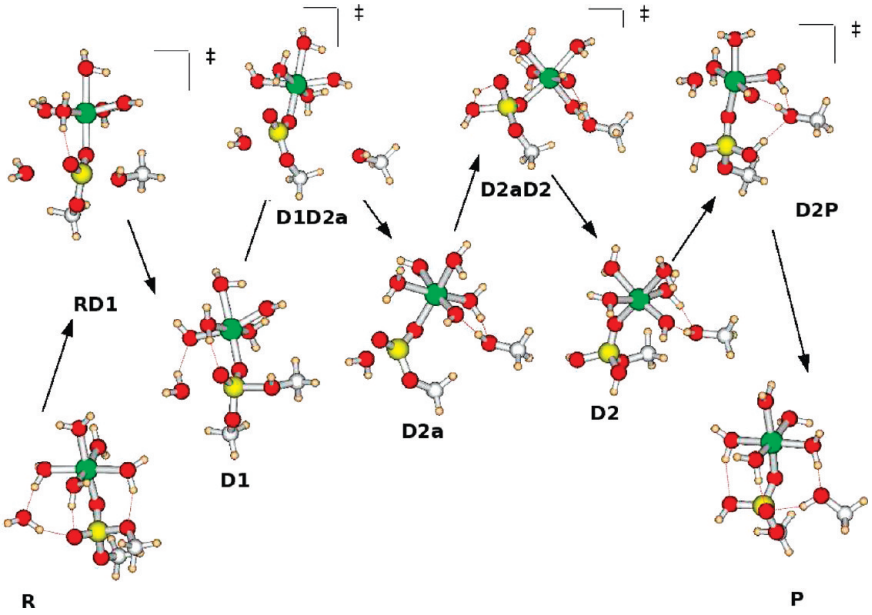

FIGURE 3: B3LYP/6-31++G(d,p) optimized stationary point structures of intermediates and transition states of the dissociative hydrolysis of dimethylphosphate complexed to pentaquo-magnesium $[DMP\text{-}Mg(H_2O)_5]^+$.

for this reaction are represented in Figures 3 and 4, and the respective energies are listed in Table 1.

The coordinates of the DFT-optimized geometries are given as Supporting Information. Selected distances of all stationary points in the different models are listed in comparison with the corresponding distances of the enzyme structures in Tables S2 and S3 of the Supporting Information. The P−O bonds are very similar in all models for tetravalent phosphorus. P−O bonds in pentavalent phosphorus are calculated to be up to ~0.1 Å shorter on the AM1/d level of theory than the DFT results. The AM1/d-calculated product state structure (preP in the enzyme) is slightly more compact than the DFT-optimized product structure in the sense that the distances to the nucleophile (P−Ow2) and to the leaving group (P−O3′) are shorter by ~0.6−0.7 Å. This shorter P−O3′ distance is observed throughout the dissociative pathway. Figures S1 and S2 show the different hydrogen bonding patterns in the optimized structures of the intermediate state D2 and the transition state D2P, optimized at the different levels. The hydrogen bond with the methanol molecule as the donor points to the magnesium-bound hydroxide ion in the vacuum models, whereas it is oriented toward O1 in the solvent model. In addition, the methanol moiety accepts a hydrogen bond from a

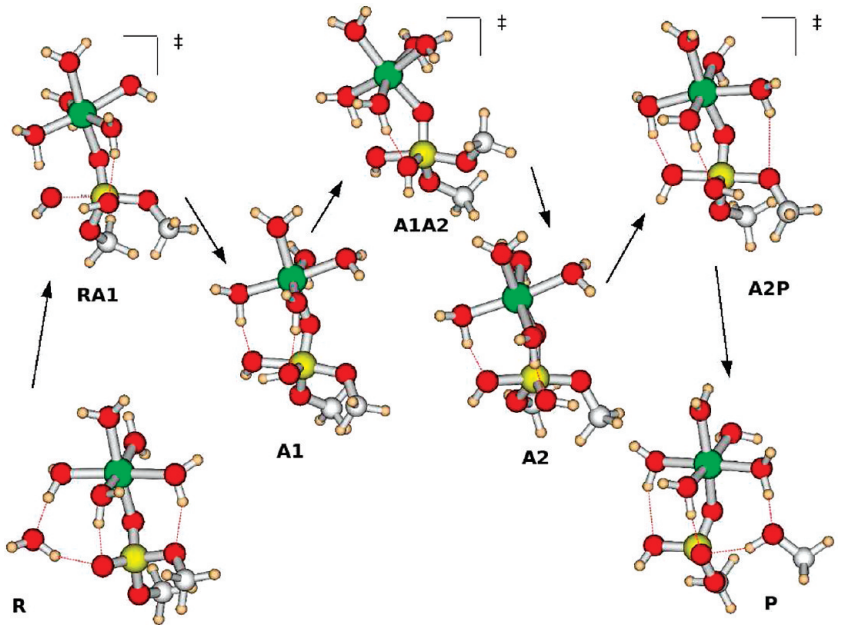

FIGURE 4: B3LYP/6-31++G(d,p)-optimized stationary point structures of intermediates and transition states of the associative hydrolysis of dimethylphosphate complexed to pentaquo-magnesium $[DMP\text{-}Mg(H_2O)_5]^+$.

Table 1: Relative Energies (kilocalories per mole) of Stationary Points along the Hydrolysis Reaction of Dimethylphosphate Complexed to Pentaquo-Magnesium $[DMP\text{-}Mg(H_2O)_5]^+$ in Vacuum and Implicit Solvent ($\varepsilon = 80$)[a]

	Dissociative							
	RD1	D1	D1D2a	D2a	D2aD2	D2	D2P	P
B3LYP/6-31++G(d,p) vacuum	54	52	60	48	63	22	24	0
B3LYP/6-31++G(d,p), $\varepsilon = 80$	54	51			72	31	32	1
AM1/d vacuum	52	48	51	48	70	11	27	6
	Associative							
	RA1	A1	A1A2	A2	A2P	P		
B3LYP/6-31++G(d,p) vacuum	37	35	39	39	39	0		
B3LYP/6-31++G(d,p), $\varepsilon = 80$	38	36	40	38	49	1		
AM1/d vacuum	37	27	37	27	36	6		

[a]For labels, see Figures 3 and 4.

magnesium-bound water molecule in the DFT-optimized structures, whereas when calculated with AM1/d, the proton bound to O2 of the phosphate forms a hydrogen bond to the methanol molecule. The proton transfer pathways follow the different orientations of the hydrogen bonds formed in state D2.

According to the AM1/d results, at the first transition state of the associative pathway, RA1, the P−Ow2 distance indicates that the new P−O bond is already formed, whereas the DFT optimization leads to a more distant nucleophile. A significant difference is observed for the transition state of the leaving group departure in the associative mechanism. The AM1/d calculations show a transition with two proton transfers. One proton moves from water molecule w1 in the direction of the leaving group oxygen, O3′, while the P−O3′ distance increases, followed by a proton transfer from O2 to O3′ and the w1 proton returning (cf. Figure S3).

The effect of the implicit solvent is a destabilization of intermediate and transition states relative to the reactant state of up to 10 kcal/mol. The energies of the first steps in the dissociative mechanism, transition state RD1 and intermediate D1, and the associative mechanism RA1, A1, are similar to the vacuum energies. This is remarkable inasmuch as the first dissociative step leads to a charge transfer to formally generate a hydroxide ion bound to the magnesium ion and a protonated phosphate group, and significant changes in charge distribution could be expected to be strongly influenced by solvent screening. However, the generation and attack of the nucleophile, dissociation of a water molecule, and P−O bond formation, as well as the intermediate state D2, formed by attack of water on the metaphosphate, and the final proton transfer to form the product, are indeed destabilized by the solvent. In the associative mechanism, the transition from the first to the second intermediate A1A2, the rotation of an OH group, is somewhat hindered in solvent relative to in vacuo. More significantly, the departure of the leaving group, which is accompanied by a proton transfer, has a 10 kcal/mol higher barrier in implicit solvent than in vacuum.

For most intermediate and transition states, the AM1/d-calculated relative energies compare well with the DFT values.

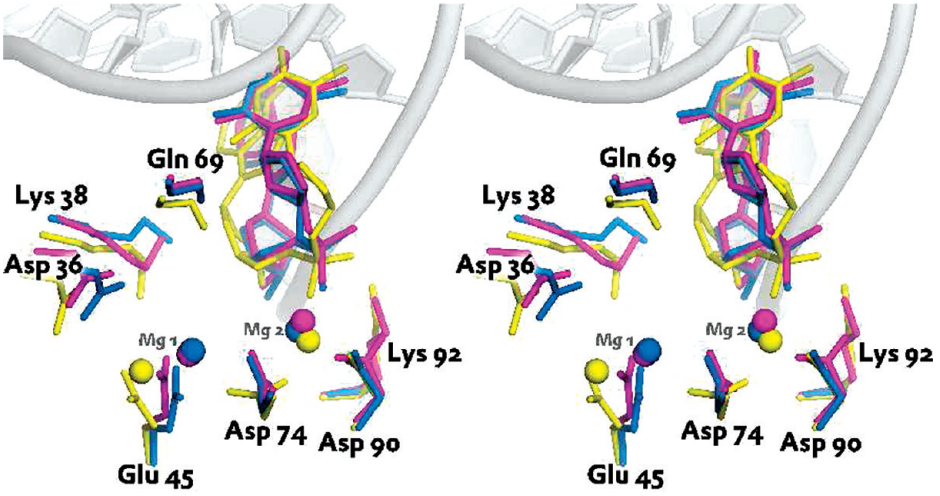

FIGURE 5: Comparison of the QM/MM-optimized reactant state structure (yellow) with crystal structures 1RVB [pink (*12*)] and 1SX8 [blue (*30*)].

With AM1/d, the associative intermediates A1 and A2 are significantly more stable than calculated at the DFT level of theory. This overstabilization of pentavalent phosphate compounds is a known error for the AM1 method (*35*), which has been alleviated by the inclusion of d-orbitals. The introduction of a pairwise scaling factor for P−O interactions has been shown (*36*) to solve this problem. However, the current standard implementation of AM1/d does not allow for extra scaling factors. The energies of the transition states in the associative mechanism agree excellently with the DFT-calculated values, as does the first step of the dissociative pathway (transition state RD1 and first dissociative intermediate D1). The barriers for the movement of the methanol moiety, step D1D2a, and the attack of water on the metaphosphate, step D2aD2, are calculated to be 7 kcal/mol higher with AM1/d than the B3LYP results. (The label D2a is used to keep the analogy of states D1 and D2 with the labels of the steps discussed in the enzymatic pathways, d1 and d2.) The semiempirically computed energy of the second dissociative intermediate, D2, is too low compared to the DFT reference. These two states show the largest discrepancies in the model calculations. The barrier for the final step in the dissociative pathway again agrees very well with the reference data.

For all models (DFT and AM1/d, vacuum and implicit solvent), the associative pathway is calculated to be energetically more favorable. The first step in the dissociative pathway, the departure of the leaving group, has a barrier which is ca. 15 kcal/mol higher than the highest-energy transition states in the associative pathway. The second step, generation and attack of the nucleophile, has an even higher barrier (63−72 kcal/mol, depending on the model). Thus, the hydrolysis of dimethylphosphate in the presence of magnesium clearly follows an associative mechanism. Moreover, a comparison to the barriers calculated for the hydrolysis of dimethylphosphate without being complexed to magnesium (*46*) shows no catalytic effect of the metal coordination.

In the enzyme, the phosphate-bound magnesium ions are coordinated by Asp and water ligands. To evaluate the performance of the AM1/d method for the competition between a monodentate and a bidentate Asp ligand, we have optimized model complexes of magnesium complexed with Asp and different numbers of water molecules at the AM1/d and B3LYP/6-31++G(d,p) levels of theory. The model systems are presented in Figure S4 of the Supporting Information. A comparison of the reaction energies computed for ligand exchange is listed in Table S4 of the Supporting Information. The AM1/d-computed reaction energies generally agree well with those obtained with DFT (ca. 4 kcal/mol error). There are two exceptions: the addition of a water ligand to the $[Mg(H_2O)_2ASP]^+$ complex, resulting in a change in the coordination number from 4 to 5, is calculated to be 7.55 kcal/mol more favorable using AM1/d. The difference in energy for the reaction from the bidentate complex $[Mg(H_2O)_3ASP]^+$ to the monodentate complex $[Mg(H_2O)_3ASP_m]^+$, changing of the coordination number from 5 to 4, is computed to be 7 kcal/mol too high at the AM1/d level of theory compared to the DFT calculation. Remarkably, at the DFT level of theory, the monodentate complex has a structure in which a proton is transferred from one water molecule to the nonligating Asp oxygen atom. The AM1/d-optimized geometry does not show such a proton-transferred structure. Proton affinities of magnesium-bound Asp were also evaluated as reaction energies of the magnesium ligating, monodentate Asp with a water molecule (cf. Table S4). The proton affinities computed at the AM1/d level agree excellently with the DFT-calculated values.

2. Enzymatic Reactant Complex. The active site atoms of the final, optimized reactant state in the protein are shown in Figure 5. Figure 5 represents a comparison of the modeled reactant state to the two crystal structures [PDB entries 1RVB (*12*) and 1SX8 (*30*)]. There are only minor differences between the two crystal structures, except for Lys92 which has been mutated to alanine in structure 1SX8 and the position of the second magnesium ion, Mg2. The side chains of Asp74 and Glu45, which coordinate Mg2, are twisted around their $C_\alpha-C_\beta$ and $C_\beta-C_\gamma$ axes, respectively, in such a way that magnesium ion Mg2 is coordinated by one carboxyl oxygen atom from each residue. In the modeled reactant state, in the QM/MM-treated subunit the scissile phosphate group is closer to the essential Asp90. The distance between the central phosphorus atom and the C_α atom of Asp90 is reduced to 6.9 Å as opposed to 7.6 Å in the crystal structure, and the distance to the side chain C_γ atom is reduced from 5.3 to 4.6 Å. These distances are similar in the other subunit of the crystal structure and the modeled complex.

The distances for the oxygen atoms coordinating magnesium ion Mg1 from the molecular dynamics (MD) simulation are plotted in Figure 6. In the first 50 ps, water molecule w2 moves, resulting in an increased distance to the scissile phosphorus

(w2−P) and a smaller water oxygen−phosphorus−leaving group oxygen angle (w2−P−O3′), thus placing w2 farther from an inline-attack geometry. Subsequently in the MD simulation, all plotted distances fluctuate only slightly around their average values, indicating that basically any snapshot from this stage of the MD simulation could serve as a starting point for further minimizations. We chose a snapshot with a w2−P distance (3.98 Å) and w2−P−-O3′ angle (117°) close to the average, the QM/MM-optimized values being 4.0 and 127°, respectively.

3. Enzymatic Product Complex. Figure 7 shows a comparison of the final optimized structure of the product state with two different crystal structures. In all crystal structures, one of the metal ions is bound to the scissile phosphate group but the structures differ significantly in the position of the second magnesium (or manganese) ion. In contrast to the other two structures, in crystal structure 1RVC (red representation in Figure 7) the second metal ion is positioned between the phosphate group and Gln69. In this structure, Glu45 is liganded to the first metal ion, whereas in structure 1SX5 (green), it binds to the second metal ion, to which it is much closer than it is to the first one. The position of the scissile phosphate group seems to follow the metal ion positions. When the metal ion is positioned more toward the Mg2 site [1RVC (red)], the phosphate rotates away from its initial position close to the thymine 3′-OH group. As suggested in ref *30*, these crystal structures can be regarded as a series moving toward the final product, from structure 1SX5, via 1STX (not shown), to 1RVC. In this picture, the modeled product state, generated from structure 1SX5 and therefore closest to this structure, can be understood as a precursor of the structures closer to the final product represented by crystal structures 1STX and 1RVC.

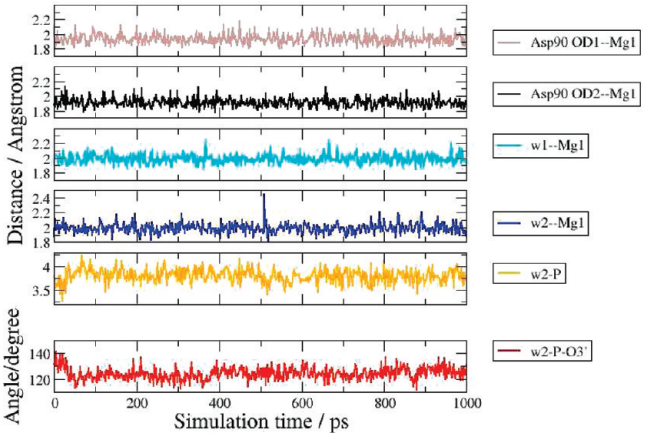

FIGURE 6: Geometric parameters during the molecular dynamics simulation: O−Mg distances of oxygen atoms of ligands coordinating magnesium ion Mg1 (top four layers), distance from nucleophile water molecule w2 to the scissile phosphorus (second from bottom,) and O−P−O angle between the attacking water molecule and the leaving group (bottom).

The main difference between the modeled complex and crystal structure 1SX5 is observed in the position of the magnesium ions. The QM/MM-optimized structure exhibits a Mg−Mg distance of 5.7 Å, whereas this is only ~3.7 Å in the crystal. The magnesium-coordinating side chains Glu45 and Asp90 are ligands with one carbonyl oxygen atom in both structures (optimized and 1SX5) but are rotated with respect to each other. This can be understood as a compromise between maintenance of the coordination sphere and the backbone conformation. The side chain of amino acid Asp74 is rotated only slightly. The scissile phosphate group has almost the same position and orientation as in crystal structure 1SX5, and the thymine leaving group is shifted by 1.2 Å with respect to the crystal structures. Residue Lys92 is almost identical in all structures, including the modeled one.

In the optimized product complex, both magnesium ions are pentacoordinated as compared to a 6-fold coordination in the reactant state (cf. Figure 5). In the case of metal ion Mg1, one Asp90 carboxyl oxygen ligand has left the ligand sphere, and Mg2 has exchanged two water molecules with one of the carboxyl oxygen atoms of Asp74.

4. Enzymatic Reaction Pathways. The pathways sketched in Figure 2 were computed together with other selected steps (not shown). Figure 8 summarizes the energies of intermediate states of the computed phosphodiester hydrolysis pathways in EcoRV and the energies of the highest transition states connecting them.

Each circle represents a minimum on the potential energy surface corresponding to a possible intermediate state of the hydrolysis reaction. The states are labeled as in Figure 2. Each line in Figure 8 represents a computed pathway between two states, and the red number on the line is the energy of the highest transition state relative to the reactant state. The result is a

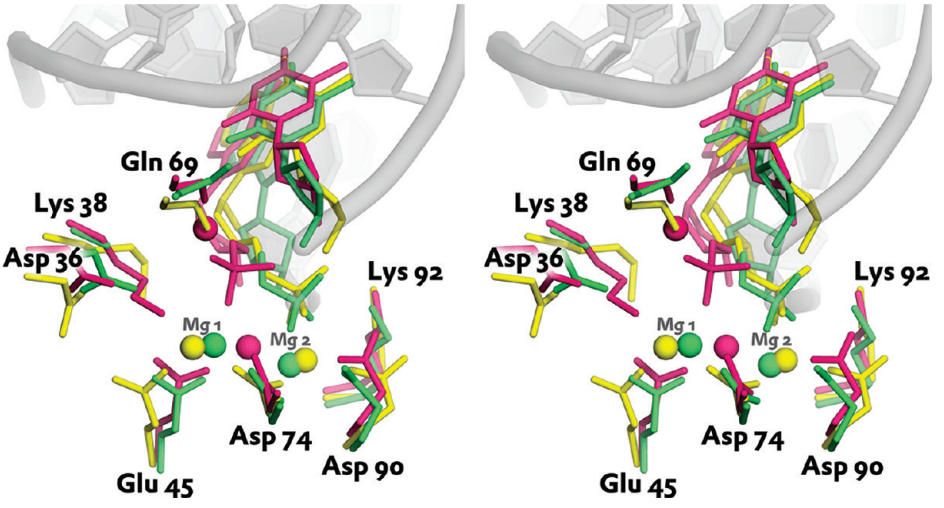

FIGURE 7: Overlay of the QM/MM-optimized product state structure (yellow) and two different crystal structures [PDB entries 1RVC (red) (*12*) and 1SX5 (green) (*30*)]. Only the active site is shown. Water molecules have been omitted for the sake of clarity.

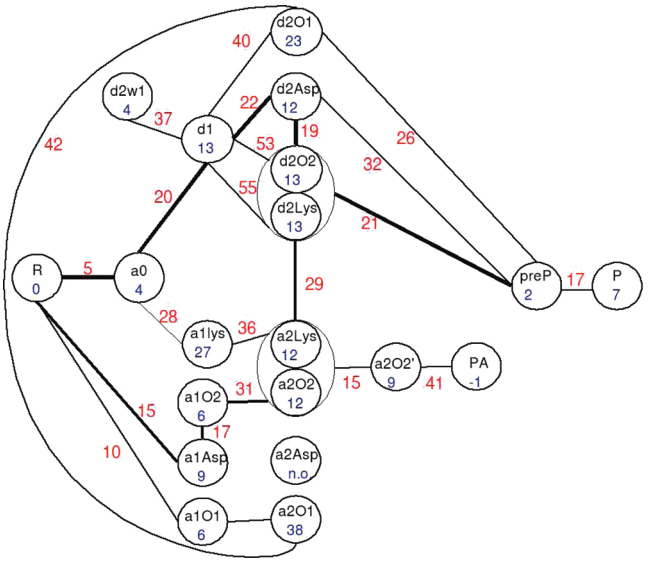

FIGURE 8: Relative energies (in kilocalories per mole) of intermediate states (blue numbers in circles) computed for the enzymatic phosphodiester hydrolysis pathways sketched in Figure 2. Two circles within an ellipse are actually the same state with two different labels which show the two possibilities of reaching it. The states are labeled according to Figure 2. The labels Asp, Lys, O1, and O2 refer to the different hydrogen atom positions, colored red, green, yellow, and blue, respectively, in Figure 2. For additional states not sketched in Figure 2 (states a0, a2o2′, PA, and d2w1), see the text. A line connecting two states (circles) denotes a transition, and the red number on the line is the energy of the respective transition state. Thick lines denote the energetically most favorable pathways. The overall most favorable pathway is that connecting reactant (R) and product (P); in this case, the energetically highest transition state has a lower energy than the energetically highest transition states of the other pathways. This is the R−a0−d1−d2Asp−d2O2/d2Lys−preP−P pathway. The highest transition state in this pathway has a relative energy of 22 kcal/mol.

complex network of pathways. Some transitions drawn in Figure 2 actually consist of multiple subtransitions due to conformational transitions. Following the lines connecting the different states from reactant (R) to product (P) provides all possible pathways for which the elementary steps have been calculated.

Whether a certain pathway is energetically feasible is determined by the energy of the highest transition state along the pathway, i.e., the highest energy point to be overcome in the whole hydrolysis reaction. In Figure 8, this pathway is highlighted with thick lines. The highest-energy transition state has a relative energy of 22 kcal/mol and connects states d1 and d2Asp. Lines of medium thickness mark the energetically second most-favorable pathway with a highest-energy transition state of 31 kcal/mol, located on the transition from state a1O2 to state a1O2.

The energetics and evolution of the geometry along the different pathways are described in the following sections.

All different pathways merge at a preproduct state denoted preP. To reach the final product state, which is more similar to the crystal structure than preP, further conformational changes must occur. These are mainly the movement of the two magnesium ions and a rearrangement of their coordination sphere. The minimum energy pathway for this final rearrangement shows one more intermediate and two transition states, of which the transition state highest in energy is 17 kcal/mol above the reactant state.

4.1. Energetically Most Favorable Dissociative Phosphodiester Hydrolysis Pathway: Dissociation and Leaving Group Protonation by w1, Generation of a Nucleophile by Transfer of a Proton to Asp90, Bond Formation, and Reprotonation. The first step along the lowest-energy pathway is a reorientation of water molecule w2 (for numbering, see Figure 9), which leaves the ligand sphere of magnesium ion Mg1 and becomes positioned inline with the scissile P−O bond at a

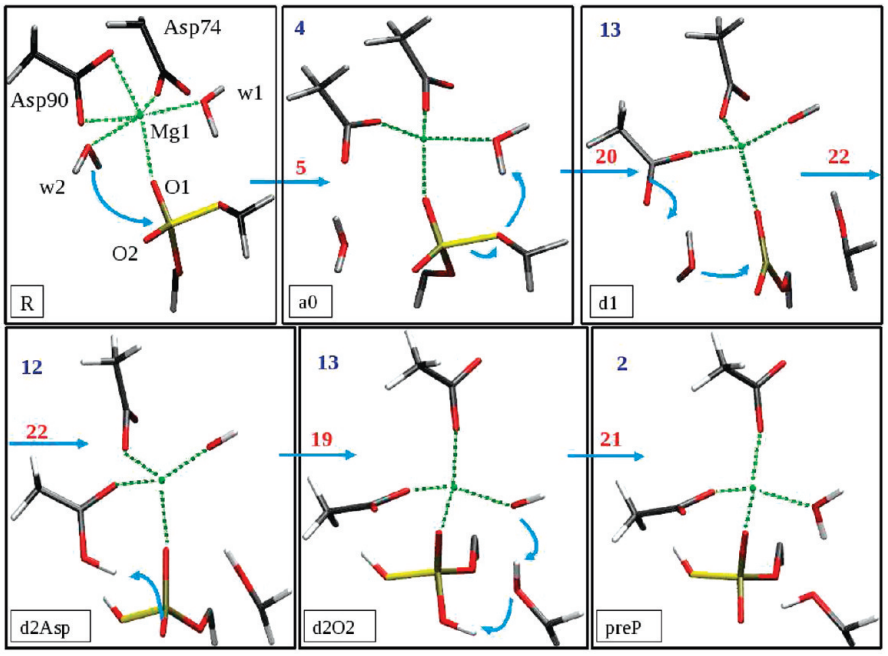

FIGURE 9: Energetically most favorable dissociative mechanisms for DNA cleavage by EcoRV. Only the most relevant atoms of the active site are shown, for the sake of clarity. Blue numbers represent energies of minima relative to the reactant state in kilocalories per mole, and red numbers indicate the energies of the highest transition states for the respective steps. The first step is an orientation of water molecule w2. The magnesium ion changes its coordination number from six to four. The transition for formation of the nucleophile by transfer of a proton from water molecule w1 to Asp90 (d1−d2Asp transition) is the highest-energy point (22 kcal/mol) in this pathway.

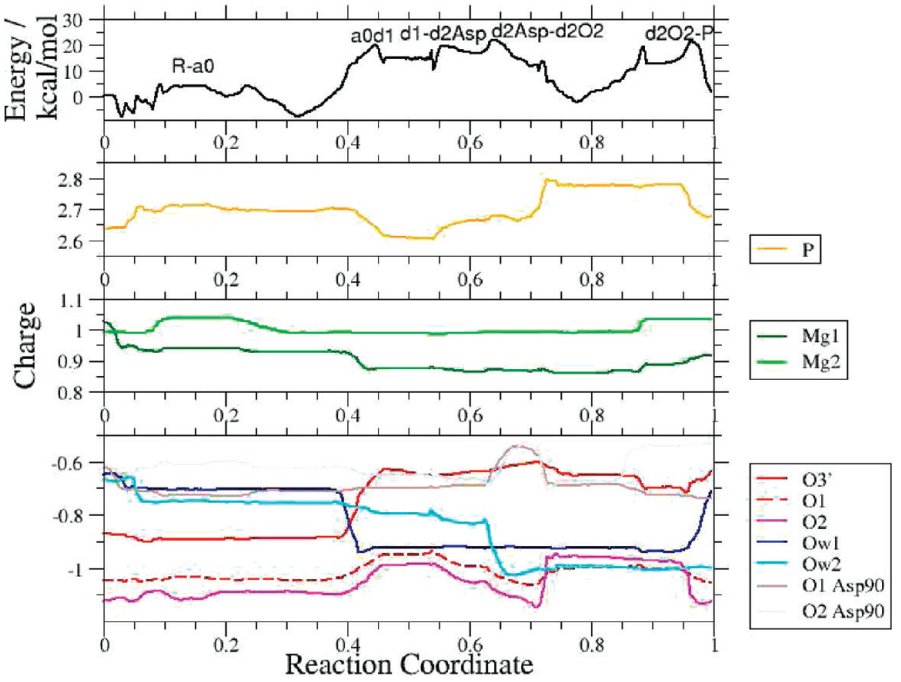

FIGURE 10: Energy profile of the dissociative pathway (top panel) and evolution of the Mulliken charges at atoms involved in bonds being formed and broken (bottom panels).

distance of 2.92 Å. At the same time, the side chain of Asp90 rotates such that one of the carboxylic oxygen atoms is no longer ligated to Mg1 but rather is hydrogen bonded to the hydroxyl group of Tyr72. The magnesium ion thus changes its coordination number from six to four and is now coordinated by one carboxylic oxygen atom from each of the side chains Asp74 and Asp90, one oxygen atom of the phosphate group, and water molecule w1 (state a0). The barrier for this preorientation step is 5 kcal/mol.

The second step (Figure 2, step Rd1) is the dissociation of the P−O bond, which is accompanied by the transfer of a proton from a magnesium-coordinated water molecule (w1) to the thymine O3′ atom. The P−O bond distances for the nucleophile and leaving group oxygen are very similar, with values of 2.79 and 2.76 Å, respectively. The transition state is 20 kcal/mol higher in energy than the reactant state and is a rather late transition state, with a structure similar to the product of this step, indicating that dissociation of the P−O bond requires more energy than proton transfer. Notably, no direct P−O bond dissociation pathway without preceding movement of water molecule w2 was found. The dissociation product has a rather low relative energy of 13 kcal/mol.

The attack of the nucleophile is the next step. The side chain of Asp90 rotates toward water molecule w2 and into hydrogen bonding distance. This hydrogen bond is maintained while w2 approaches the phosphorus atom to a distance of ca. 1.8 Å until one proton of w2 is transferred to the carboxylic group of Asp90 (Figure 2, d1−d2Asp step). The transition state energy for this concerted nucleophile generation and nucleophilic attack is 22 kcal/mol.

Two further proton transfer steps regenerate the protonation states of the catalytic residues. First, a proton is transferred from Asp90 to O2 of the phosphate group (d2Asp−d2O2 step in Figure 2 or 9), and in a second process, two protons move concertedly: one from the phosphate oxygen to the leaving group oxygen and the other from the leaving group oxygen to hydroxide ion w1 (d2O2−P step in Figure 2 or d2O2−preP step in Figure 9). The highest-energy transition state for these reprotonation steps lies 21 kcal/mol higher than the reactant state.

A direct reprotonation of water molecule w1 by transfer of a proton from Asp90 is found to be less favorable than the double proton transfer and has a transition state energy of 31 kcal/mol.

The energy profile of the whole pathway is shown in the top panel of Figure 10. The other panels in Figure 10 show how the Mulliken charges on the phosphorus atom, the magnesium ions, and the most important oxygen atoms evolve during the course of the reaction. The most striking transition in terms of charges takes place at the reaction coordinate (RC) value of ca. 0.4: here, the oxygen atom of water molecule w1 (Ow1) becomes much more negatively charged while the O3′ atom of the leaving group becomes less negative by approximately the same amount (RC = 0.39). This step accompanies the transfer of a proton from water molecule w1 to the leaving group. The formation of the nucleophile can also be observed in the charge of the Ow2 atom becoming more negative, while the proton acceptor, the oxygen atom of Asp90, loses negative charge (RC = 0.61). The formation of the new P−O bond does not change the charge of the oxygen atom, but the charge of the phosphorus atom increases. Transfer of a proton from Asp90 to the phosphate O2 atom (RC ≈ 0.67) is also accompanied by corresponding charge shifts. The reprotonation of water molecule w1 takes place at a reaction coordinate of ca. 0.98 and is reflected by the charge of atom Ow1 becoming less negative and the atom O2, the atom from which the proton is transferred, changing back to its original charge.

Other interesting transitions are also reflected in the changes of the Mulliken charges. The change in the magnesium ligand sphere from six to five, and then to four coordination partners, is reflected in decreases in the charges of the coordinating oxygen atoms, O1 of Asp90 and Ow2. The charge of magnesium ion Mg1, however, decreases only with the loss of the first ligand, the aspartate oxygen atom. Interestingly, the "missing" positive charge is transferred to the phosphorus atom. The formation

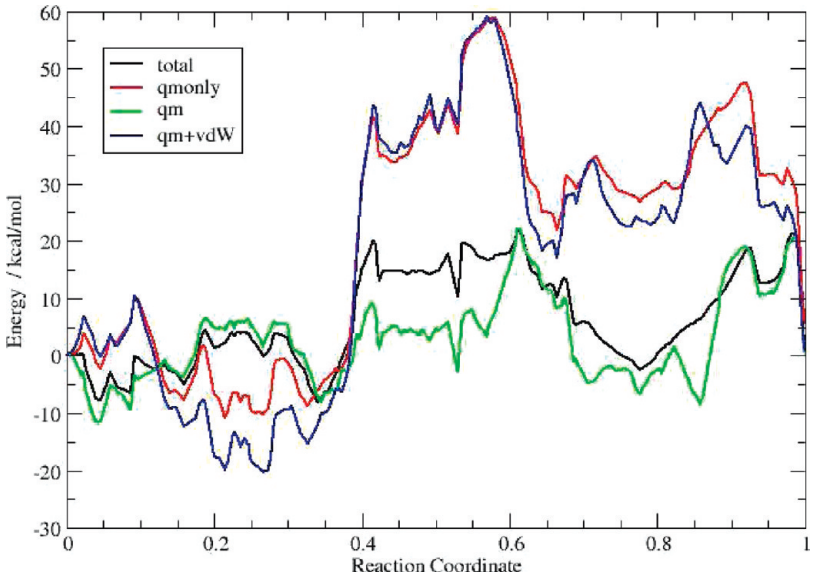

FIGURE 11: Reaction profile dissected into different energy contributions: black, total energy; red, QM energy of the QM region alone; blue, QM energy of the QM region with uncharged MM atoms around [QM energy plus van der Waals interactions of the QM atoms with the MM atoms (and MM with MM)]; green, energy of the quantum mechanically (QM) treated part in the field of the molecular mechanically treated (MM) atoms, but no van der Waals interaction at all and no electrostatic interaction within the MM atoms. The coordinates are the same in all curves; only the energy contributions considered are different.

of the metaphosphate after dissociation step d1 leads to less polarization of the phosphate group: the phosphorus atom and atoms O1 and O2 become less charged. At this point, the magnesium ion undergoes its second change to a less positive charge.

Figure 11 shows the energy profile of the reaction decomposed into different parts. A comparison of the energy profile calculated with the QM part only (red curve) and the energy profile calculated for QM energy plus additional van der Waals interactions, i.e., no electrostatic interaction between MM atoms (blue), shows that the geometric template given by the protein does not change the reaction profile significantly. In contrast, the electrostatic interactions with the protein atoms reduce significantly the heights of the high barriers as can be seen from the difference between the energy profile computed for the QM part with (green) and without (red) taking the surrounding protein atoms into account. A comparison with Figure 10 reveals that these barriers are associated with a significant amount of charge being shifted around, e.g., by proton transfer. Between RC values of ≈0.1 and ≈0.4, mainly conformational changes take place, without causing significant charge differences, which can also be seen in Figure 10. At this stage of the reaction, the steric effect of the protein is favorable as one can see from the comparison of the energies of the QM atoms alone (red) and with the addition of van der Waals interactions (blue).

4.2. Energetically Most Favorable Associative Phosphodiester Hydrolysis Pathway: Generation of the Nucleophile by Transfer of a Proton to Asp90, Association, Bond Cleavage and Leaving Group Protonation by w1, and Reprotonation. The associative pathway with the lowest overall barrier also requires Asp90 as a general base for abstraction of a proton from water molecule w2. The proton-accepting oxygen atom loses its coordination to the magnesium ion, resulting in 5-fold coordination. This first step (R−a1Asp) has a barrier of 11 kcal/mol and is followed by further transfer of the proton to atom O2 with a transition state at 15 kcal/mol (a1Asp−a1O2). The hydroxide ion remains bound to the Mg^{2+} ion during the second proton transfer. Upon attack of the nucleophile on the scissile phosphorus, the hydroxide ion leaves the ligand sphere of the Mg^{2+} ion which is then tetracoordinated. The transition state for the formation of the associative pentavalent phosphorus intermediate has an energy of 31 kcal/mol. The new P−O bond is already formed with a length of ca. 1.7 Å at the transition state, and the O−Mg distance is 2.64 Å. At this point, the hydroxide ion has left the magnesium coordination sphere which has not been rearranged. The associative intermediate has a trigonal bipyramidal configuration with similar lengths of both axial P−O bonds (1.70 and 1.69 Å) and is 12 kcal/mol less stable than the reactant state. The formation of this intermediate is the rate-determining step in this pathway.

The departure of the leaving group has a transition state with an energy similar to that of the transition state of the attack step (29 kcal/mol above the reactant state energy). At the transition state, the P−O3′ distance is 1.82 Å. The leaving group is protonated by transfer of a proton from water molecule w1 as already described for the dissociative pathway (a2O2−d2O2 step). The final steps of this mechanism, which are the reformation of intermediate d2O2, reprotonation, and conformational changes, are identical to those of the energetically most favorable dissociative phosphodiester hydrolysis pathway described above.

4.3. Energetically Second Most Favorable Associative Phosphodiester Hydrolysis Pathway: Nucleophile Generation by Transfer of a Proton to O2 via Lys92, Association, Bond Cleavage and Leaving Group Protonation by w1, and Reprotonation. The first step in the energetically second most favorable associative pathway is the same as for the dissociative pathway described above: water molecule w2 leaves the Mg^{2+} ligand sphere and approaches the scissile phosphate. From this intermediate, the hydroxide ion forms by a sequential two-proton transfer step: one proton of the NH_3^+ group from Lys92 is transferred to the unbound oxygen of the scissile phosphate group, O2, and a second proton from water molecule w2 is transferred to Lys92, reprotonating it. In concert with the proton

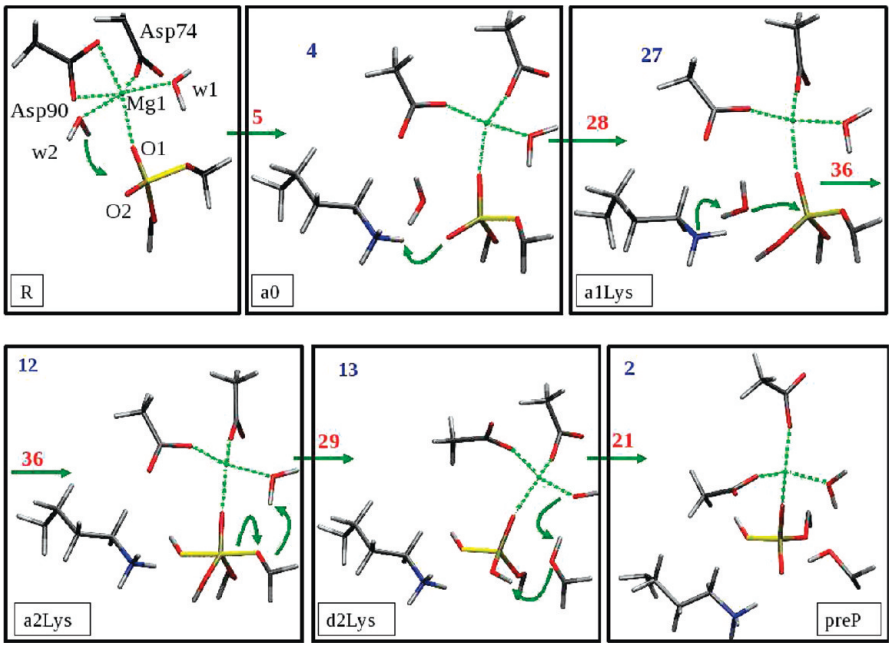

FIGURE 12: Energetically second most favorable associative mechanism for DNA cleavage by EcoRV. Only the most relevant atoms of the active site are shown for the sake of clarity. Blue numbers represent energies of minima relative to the reactant state in kilocalories per mole, and red numbers indicate the energies of the highest transition states for the respective step. The first step is the positioning of the nucleophile in-line for attack, as in the dissociative pathway. The hydroxide ion is generated by a relay transfer of a proton from water molecule w2 to the phosphate group via Lys92. The step that includes attack of the nucleophile and formation of the associative intermediate has the highest transition state energy (36 kcal/mol) in this pathway.

transfer is the attack of the nucleophile and formation of the new O−P bond. The associative intermediate (Figure 12, a2Lys) is identical with the corresponding associative intermediate of the energetically most favorable associative pathway described above (Figure 13, a2O2). The transition state energy is 36 kcal/mol above the reactant state energy. In comparison, a transition from preoriented intermediate a0 to associative intermediate a2O2 with direct transfer of a proton from water molecule w2 to the phosphate O2 atom has a barrier of 45 kcal/mol.

4.4. Pathways with Transfer of a Proton to O1. Transfer of a proton from water molecule w2 to atom O1 as a first step (R−a1O1) can easily be achieved over a barrier of 10 kcal/mol. However, the subsequent nucleophilic attack requires significantly more energy (41 kcal/mol). The formation of the preproduct from this intermediate is not direct but via state d2O1. The barrier for this transition to the preproduct state is also 41 kcal/mol.

Approximately the same barrier height is found for the dissociative pathway via atom O1 protonation: 40 kcal/mol for the transition state with the transfer of a proton to atom O1 and the attack of w2 (as a hydroxide ion) at the phosphorus at the second step after P−O bond dissociation (d1−d2O1). The final transfer of a proton from O1 to (hydroxide) w1 forming the preproduct state preP has a barrier of 26 kcal/mol.

4.5. Other Pathways. After cleavage of the P−O bond and formation of a metaphosphate intermediate (step Rd1), either water molecule w1 or w2 could in principle act as the nucleophile and attack the phosphorus atom. Generation of a hydroxide ion from water molecule w2 and its attack lead to the dissociative, energetically best pathway. Water molecule w1 has already donated a proton to the leaving group and has thus been transformed to a hydroxide ion ready for nucleophilic attack. The barrier for this attack, however, is 36 kcal/mol, significantly higher than the barrier for attack of water molecule w2.

The associative intermediate a2O2 can undergo pseudorotation over a transition state with an energy of 15 kcal/mol, to form another trigonal bipyramidal intermediate (denoted a2O2′ in Figure 8) which possesses atoms O2 and O5′ at the apical positions. This configuration is a potential precursor for dissociation of the P−O5′ bond. However, the barrier for the transfer of a proton from atom Ow2 to atom O5′ and departure of the adenosine moiety as the leaving group (leading to state PA) is 41 kcal/mol. This is comparable to the P−O3′ cleavage of associative intermediate a2O2 with direct transfer of a proton from the pentavalent phosphate moiety to the leaving group. The reason for the huge barrier is that in the a2O2′ state, there is no nearby Mg-activated water molecule to protonate the leaving group and thus lower the barrier for cleavage of the P−O5′ bond.

No stable intermediate a2Asp could be located. This state would have to be generated by transfer of a proton from w2 to Asp90 and attack of the nucleophilic hydroxide ion on the phosphate group to form a pentavalent intermediate. The pentavalent phosphate would then carry a formal charge of −2, whereas Asp90 would be neutral. However, this protonation state is apparently not stable.

Furthermore, no intermediate with a protonated metaphosphate could be trapped: all attempts to move protons from Lys92 to the metaphosphate failed, indicating that the positive charge is better stabilized by the amino group of Lys92 than by the metaphosphate.

4.6. Pathway to the Product Complex. All pathways described above merge in the preproduct state, preP. As depicted in Figure 8, further transitions lead to the final optimized product state, P. The main differences between preP and P are the position of the magnesium ions and a rotation of the phosphate group. The transition between the two states consists of two steps shown in Figure 14. First, Mg1 moves toward the carbonyl oxygen atom of Ile91, resulting in 5-fold coordination. Then, water molecule

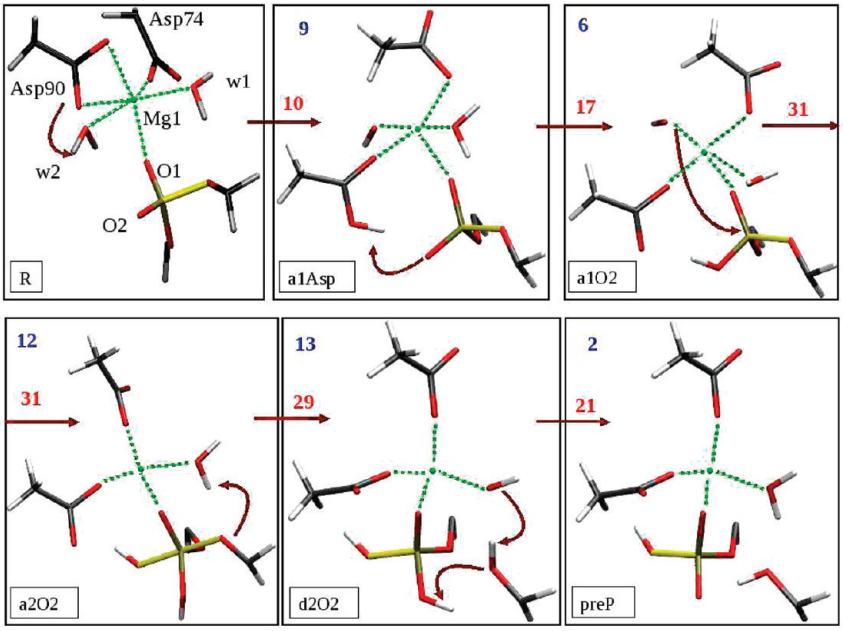

FIGURE 13: Energetically most favorable associative mechanism for DNA cleavage by EcoRV. Only the most relevant atoms of the active site are shown for the sake of clarity. Blue numbers represent energies of minima relative to the reactant state in kilocalories per mole, and red numbers indicate the energies of the highest transition states for the respective step. The first step is the generation of the nucleophile by transfer of a proton from water molecule w2 to Asp90 associated with a change in the magnesium ion coordination number from six to five. This coordination number is further reduced to four upon nucleophilic attack of water molecule w1 on the phosphorus. The formation of the associative intermediate is the rate-determining step (31 kcal/mol) in this pathway.

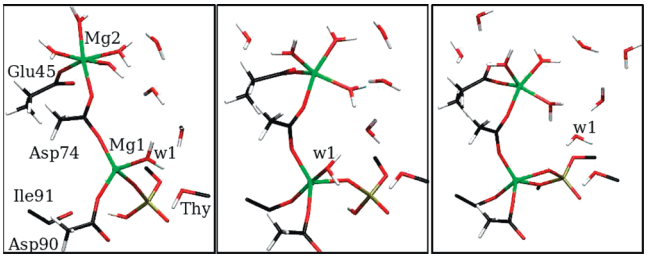

FIGURE 14: Pathway from the preproduct (left) to the product state (right). First, magnesium ion Mg1 is shifted toward the carbonyl group of Ile91, which becomes an additional ligand, changing the coordination number from four to five. Additionally, magnesium ion Mg2 loses a water ligand, reducing its coordination number to five. Furthermore, Mg2 is positioned closer to Mg1. In the second step, the phosphate group rotates in such a way that the OH group coordinates to magnesium ion Mg1 in exchange with water molecule w1.

w1 leaves the ligand sphere of magnesium ion Mg1. Upon rotation of the scissile phosphate group, the terminal oxygen atom of the phosphate group enters the ligand sphere of Mg1. Metal ion Mg2 moves closer to Mg1, exchanging two water molecules with one carboxyl oxygen of Asp74. The final coordination number of both ions is five. The two transition states of the ligand exchange reactions have similar energies, 16 and 17 kcal/mol, respectively. The final product is slightly higher in energy than the reactant state (by 5 kcal/mol), and the preproduct, preP, is marginally more stable (−2 kcal/mol) than the reactant state.

DISCUSSION

We have computed several pathways for phosphodiester cleavage in the backbone of DNA by the restriction enzyme EcoRV. Comparison of the transition state energies for the various steps indicates that two pathways are most likely, one with more dissociative and one with more associative character. Of the two, the dissociative pathway has lower transition state energies. Given the approximations in the model (involving treatment of the QM region semiempirically, computing minimum potential energy pathways, i.e., not including entropic contributions, implicit treatment of solvent water), the 9 kcal/mol difference in the highest-energy transition state should be considered highly suggestive while not completely ruling out the associative pathway.

It is important to determine which of the computed pathways agrees with existing experimental data.

A crucial step in the computed energetically favorable reaction pathways (both associative and dissociative) is the preorientation of attacking water molecule w2, in-line with the scissile P−O bond. The movement of this water molecule leads to a substantial change in the ligand sphere of Mg^{2+} ion Mg1, the coordination number of which is reduced from six to four. This finding yields a possible explanation for the selectivity of EcoRV for certain divalent cations (*5*, *14*, *21*). While the "active" metals Mg, Mn, and Co all readily change their coordination number from six to four, the larger metal ion Ca^{2+} is highly unlikely to be only tetracoordinated. Replacement of Mg1 with Ca^{2+} thus would block the initial preorientation step, leading to much higher barriers for subsequent nucleophile attack and P−O bond cleavage. The second metal ion, however, remains hexacoordinated during the cleavage reaction and could be replaced with Ca^{2+}. Since the precise position of this second metal ion seems to be less important, the increased metal ion− metal ligand distances when substituting Mg^{2+} with Ca^{2+} would not hinder cleavage. In this light, the experimental finding that EcoRV with mixed cofactors (Mn and Ca) cleaves DNA (*21*) would be consistent with the Ca^{2+} ion being positioned at the less critical Mg2 site, whereas the Mg1 site would be occupied by Mn^{2+} ions.

The pH dependence of the reaction rate has been measured and shows a Gaussian pH profile with a maximum at pH 8.5 (*14*). This has been interpreted as indicating the presence of two

essential titratable groups and two proton transfers in the catalytic step, i.e., general base catalysis of the attack of the hydroxide ion and general acid catalysis of the expulsion of the leaving group (*14*). The two energetically most favorable pathways, both the dissociative one and the associative one, show exactly these steps. (1) Asp90 accepts a proton from water molecule w2, thus generating a hydroxide nucleophile, and (2) the leaving group is protonated by water molecule w1. However, a difference between the associative and dissociative pathways is that for the dissociative pathway, the generation and attack of the nucleophile is the step with the highest-energy transition state of the whole pathway, although the departure of the leaving group also has a transition state similar in energy. In the associative pathway, however, the hydroxide ion is formed with a significantly lower barrier and the nucleophilic attack has the highest-energy transition state. Again, the leaving group departure is close in energy to the attack step. The general base-catalyzed nucleophile generation has a rather low barrier, and therefore, this proton transfer step is unlikely to explain the strong pH dependence of the reaction rate. Thus, the pH dependence favors a pathway with a more dissociative character.

Mutation experiments have shown Lys92 to be essential and, moreover, have demonstrated a requirement for a positive charge at the site of the Lys92 amino group (*30*). The calculations do not include a direct catalytic role of amino acid Lys92, and the pathway which involves Lys92 in a proton relay is rather unlikely from an energetic point of view. However, a possible role of Lys92 is to ensure proper binding and bending of the DNA. Correct positioning of the scissile phosphate by formation of hydrogen bonds to the nonbridging phosphate oxygen and the phosphate group next in sequence seems to be more effective than electrostatic attraction of the negatively charged phosphate group by a positive charge such as the sodium ion observed in the crystal structure of the K92A mutant (*30*). The proper orientation of the scissile phosphate group is more important in the dissociative case, in which the intermediate metaphosphate can in principle rotate and thus inhibit attack of the nucleophile, whereas the pentavalent intermediate is held by its two backbone bonds.

Consistent with the catalytic function of EcoRV, the computed reaction pathways in the enzyme are energetically more favorable than in the small molecule models. The more likely enzymatic pathway has more dissociative character, whereas in vacuum and (implicit) solution, the associative mechanism is preferred. The initial step of the dissociative pathway is the departure of the leaving group associated with the transfer of a proton from a magnesium-bound water molecule. This takes place in both the model system and the enzymatic pathway, both of which contain the functional groups involved in this catalytic step. However, the dissociative intermediate (as well as the barrier) is significantly stabilized by the enzyme, mainly by electrostatic interaction. Both the dissociative and associative pathways require the generation of an attacking hydroxide ion. The enzyme enhances OH^- generation by transfer of a proton to Asp90, whereas the small molecule system allows only direct transfer of a proton to the phosphate group. General base catalysis by Asp90 in the enzyme is facilitated by reorientation of water molecule w2, and Asp90 also leaving the coordination sphere of the magnesium ion prior to the proton transfer step. With regard to the associative pathway, a lowering of energy barriers by the enzyme is achieved in an alternative mechanism, via Asp90, which is not possible in the small molecule system. Comparison of the reaction mechanism in the model system to the more similar, second energetically most favorable, associative pathway (via Lys92) shows no significant change in energy barrier, and hence no catalytic effect by the enzyme.

On the basis of several crystal structures (*12*, *27*, *30*), a catalytic model has been proposed in which these three binding sites are occupied at different steps of the mechanism. In this model, the metal position directly at the scissile phosphate is occupied upon binding of the DNA to the protein. The second step involves a significant conformational change of the scissile phosphate, movement of the metal ion from the Asp90/Asp74 site to the Asp74/Glu45 site, and binding of an additional metal ion at the third metal binding site, ligated by the scissile phosphate group of Asp74, resulting in the preattack conformation of a classical two-metal mechanism (*30*). The suggested conformational change, prior to cleavage, is consistent with the crystal structure of the K38A mutant−DNA product complex, in which two metal ions bind directly to the cleaved, shifted 5′-phosphate. According to ref *30*, the transition to this hitherto unobserved conformation is hindered by crystal packing effects and could be made visible only in a different crystal form. A short molecular dynamics simulation (*5*) exhibited a spontaneous conformational transition of the scissile phosphate group after a simulation time of 150 ps, consistent with the catalytic model described above, involving a twist of the scissile phosphate group and movement of the metal ions. In contrast to the simulation result described above, in the present (1 ns) MD simulation with full solvation, neither twist of the scissile phosphate group nor significant movement of the metal ions was observed. Furthermore, another, significantly longer, 50 ns molecular dynamics simulation of the reactant complex was performed, and again, no such conformational transition was observed (data not shown). Hence, this transition is unlikely to happen rapidly and spontaneously. Indeed, the reaction pathways computed starting from a reactant state which is similar to the crystal structures of the wild type and the K92A mutant show that the cleavage reaction can occur without significant prior conformational transitions. However, we have also examined whether rotation of the scissile phosphate group together with some rearrangement of the metal ions is energetically accessible after the hydrolysis step itself (pathway to the product complex, preP to P), and this transition was indeed found to have a feasible barrier. Thus, the crystallographically observed K38A mutant product complex (PDB entry 1STX) with the twisted scissile phosphate group may arise from rotation of the phosphate around the remaining O−C bond after cleavage. Crystal structures of this mutant in the other space group, *P*1 (PDB entry 1SX5), and of the wild type (PDB entry 1RVC) show a scissile phosphate group which is rotated even more from its position in the reactant state, together with, in case of the wild-type structure, significantly altered metal ion positions. It would be most helpful if a crystal structure of a reactant state with a twisted phosphate group could be determined.

CONCLUSIONS

In this work, pathways for the hydrolysis reaction of the phosphodiester backbone of DNA in the restriction enzyme EcoRV are reported. An extensive network of reaction pathways was generated, from which the most probable and alternative reaction mechanisms were identified. The most likely pathway has a more dissociative than associative character, consistent with several experimental observations. The departure of the

leaving group is facilitated by transfer of a proton of a magnesium-activated water molecule. From the comparison with small molecule systems, the following catalytic effects of the protein can be deduced: The active site arranges the scissile phosphate group such that the magnesium-coordinated water molecules can directly contribute to catalysis. An aspartate residue, which, by coordination to the essential magnesium metal ion, is ideally positioned, acts as a general base and accepts a proton to generate the nucleophile. The electrostatic environment provided by the protein reduces the barriers for those catalytic steps in which charge is transferred (e.g., as protons).

ACKNOWLEDGMENT

P.I. is grateful to Sonja M. Schwarzl and Frank Noé for helpful discussions and assistance with charge scaling and parameter fitting. We also thank Thomas Splettstösser for help with the stereo figures.

SUPPORTING INFORMATION AVAILABLE

AM1/d parameters for phosphorus, selected distances of stationary points along the hydrolysis reaction for the small molecule model system and optimized geometries, and figures of selected stationary points, optimized at different levels of theory. This material is available free of charge via the Internet at http://pubs.acs.org.

REFERENCES

1. Schildkraut, I., Banner, C., Rhodes, C. S., and Parekh, S. (1984) The Cleavage Site for the Restriction Endonuclease *Eco*RV is 5′-GAT/ATC-3′. *Gene 27*, 327–329.
2. Williams, N. H., Takasaki, B., Wall, M., and Chin, J. (1999) Structure and Nuclease Activity of Simple Dinuclear Metal Complexes: Quantitative Dissection of the Role of Metal Ions. *Acc. Chem. Res. 32*, 485–493.
3. Kovall, R. A., and Matthews, B. W. (1999) Type II Restriction Endonucleases: Structural, functional and evolutionary relationships. *Curr. Opin. Chem. Biol. 3*, 578–583.
4. Perona, J. J. (2002) Type II restriction endonucleases. *Methods 28*, 353–364.
5. Baldwin, G. S., Sessions, R. B., Erskine, S. G., and Halford, S. E. (1999) DNA Cleavage by the *Eco*RV Restriction Endonuclease: Roles of Divalent Metal Ions in Specificity and Catalysis. *J. Mol. Biol. 288*, 87–103.
6. Groll, D. H., Jeltsch, A., Selent, U., and Pingoud, A. (1997) Does the Restriction Endonuclease *Eco*RV Employ a Two-Metal-Ion Mechanism for DNA Cleavage? *Biochemistry 36*, 11389–11401.
7. Halford, S. E., and Goodall, A. J. (1988) Modes of DNA Cleavage by the *Eco*RV Restriction Endonuclease. *Biochemistry 27*, 1771–1777.
8. Horton, N. C., Otey, C., Lusetti, S., Sam, M. D., Kohn, J., Martin, A. M., Ananthnarayan, V., and Perona, J. J. (2002) Electrostatic Contributions to Site Specific DNA Cleavage by *Eco*RV Endonuclease. *Biochemistry 41*, 10754–10763.
9. Horton, N. C., Connolly, B. A., and Perona, J. J. (2000) Inhibition of *Eco*RV Endonuclease by Deoxyribo- 3′-S-phosphorothiolates: A High-Resolution X-ray Crystallographic Study. *J. Am. Chem. Soc. 122*, 3314–3324.
10. Horton, N. C., and Perona, J. J. (1998) Recognition of Flanking DNA Sequences by *Eco*RV Endonuclease Involves Alternative Patterns of Water-mediated Contacts. *J. Biol. Chem. 273*, 21721–21729.
11. Horton, N. C., and Perona, J. J. (1998) Role of Protein-induced Bending in the Specificity of DNA Recognition: Crystal Structure of *Eco*RV Endonuclease Complexed with d(AAAGAT)−d(ATCTT). *J. Mol. Biol. 277*, 779–787.
12. Kostrewa, D., and Winkler, F. K. (1995) Mg^{2+} Binding to the Active Site of *Eco*RV Endonuclease: A Crystallographic Study of Complexes with Substrate and Product DNA at 2 Å Resolution. *Biochemistry 34*, 683–696.
13. Parry, D., Moon, S. A., Liu, H.-H., Heslop, P., and Connolly, B. A. (2003) DNA Recognition by the *Eco*RV Restriction Endonucleases Probed using Base Analogues. *J. Mol. Biol. 331*, 1005–1016.
14. Sam, M. D., and Perona, J. J. (1999) Catalytic Roles of Divalent Metal Ions in Phosphoryl Transfer by *Eco*RV Endonuclease. *Biochemistry 38*, 6576–6586.
15. Stanford, N. P., Halford, S. E., and Baldwin, G. S. (1999) DNA cleavage by the *Eco*RV restriction endonuclease: pH dependence and proton transfers in catalysis. *J. Mol. Biol. 288*, 105–116.
16. Thomas, M. P., Brady, R. L., Halford, S. E., Sessions, R. B., and Baldwin, G. S. (1999) Structural analysis of a mutational hot-spot in the *Eco*RV restriction endonuclease: A catalytic role for a main chain carbonyl group. *Nucleic Acids Res. 27*, 3438–3445.
17. Sam, M. D., and Perona, J. J. (1999) Mn^{2+}-dependent Catalysis by Restriction Enzymes: Pre-Steady-State Analysis of *Eco*RV Endonuclease Reveals Burst Kinetics and the Origins of Reduced Activity. *J. Am. Chem. Soc. 121*, 1444–1447.
18. Baldwin, G. S., Vipond, I. B., and Halford, S. E. (1995) Rapid Reaction Analysis of the Catalytic Cycle of the *Eco*RV Restriction Endonuclease. *Biochemistry 34*, 705–714.
19. Connolly, B. A., Eckstein, F., and Pingoud, A. (1984) The Stereochemical Course of the Restriction Endonuclease *Eco*RI-catalyzed Reaction. *J. Biol. Chem. 259*, 10760–10763.
20. Erskine, S. G., Baldwin, G. S., and Halford, S. E. (1997) Rapid-Reaction Analysis of Plasmid DNA Cleavage by the *Eco*RV Restriction Endonuclease. *Biochemistry 36*, 7567–7576.
21. Vipond, I. B., Baldwin, G. S., and Halford, S. E. (1995) Divalent Metal Ions at the Active Site of the *Eco*RV and *Eco*RI Restriction Endonucleases. *Biochemistry 34*, 697–704.
22. Pingoud, A., and Jeltsch, A. (2001) Structure and function of type II restriction endonucleases. *Nucleic Acids Res. 29*, 3705–3727.
23. Winkler, F. K., Banner, D. W., Oefner, C., Tsernoglou, D., Brown, R. S., Heatman, S. P., Bryan, R. K., Martin, P. D., Petratos, K., and Wilson, K. S. (1993) The crystal structure of *Eco*RV endonuclease and of its complexes with cognate and non-cognate DNA fragments. *EMBO J. 12*, 1781–1795.
24. Horton, N. C., and Perona, J. J. (2000) Crystallographic snapshots along a protein-induced DNA-bending pathway. *Proc. Natl. Acad. Sci. U.S.A. 97*, 5729–5734.
25. Selent, U., Rüter, T., Köhler, E., Liedtke, M., Thielking, V., Alves, J., Oelgeschläger, T., Wolfes, H., Paters, F., and Pingoud, A. (1992) A Site-directed Mutagenesis study To Identify Amino Acid Residues Involved in the Catalytic Function of the Restriction Endonuclease *Eco*RV. *Biochemistry 31*, 4808–4815.
26. Horton, N. C., Newberry, K. J., and Perona, J. J. (1998) Metal ion-mediated substrate-assisted catalysis in type II restriction endonucleases. *Proc. Natl. Acad. Sci. U.S.A. 95*, 13489–13494.
27. Perona, J. J., and Martin, A. M. (1997) Conformational Transitions and Structural Deformability of *Eco*RV Endonuclease Revealed by Crystallographic Analysis. *J. Mol. Biol. 273*, 207–225.
28. Martin, A. M., Horton, N. C., Lusetti, S., Reich, N. O., and Perona, J. J. (1999) Divalent metal dependence of site-specific DNA binding by the *Eco*RV restriction endonuclease. *Biochemistry 38*, 8430–8439.
29. Vipond, I. B., and Halford, S. E. (1995) Specific DNA recognition by *Eco*RV Restriction Endonucleases Induced by Calcium Ions. *Biochemistry 34*, 1113–1119.
30. Horton, N. C., and Perona, J. J. (2004) DNA Cleavage by *Eco*RV Endonuclease: Two Metal Ions in Three Metal Ion Binding Sites. *Biochemistry 43*, 6841–6857.
31. Frey, P. A. (1989) Chiral Phosphorothioates: Stereochemical Analysis of Enzymatic Substitution at Phosphorus. In Advances in Enzymology and Related Areas of Molecular Biology (Meister, A., Ed.) Vol. 62, pp 119−201, Wiley-VCH, Berlin.
32. Burgers, P. M. J., Eckstein, F., Hunnermann, D. H., Baraniak, J., Kinas, R. W., Lesiak, K., and Sted, W. J. (1979) Stereochemistry of hydrolysis of adenosine 3′:5′-cyclic phosphorothioate by the cyclic phosphodiesterase from beef heart. *J. Biol. Chem. 254*, 9959–9961.
33. Ahlrichs, R., Bar, M., Haser, M., Horn, H., and Kolmel, C. (1989) Electronic Structure Calculations on Workstation Computers: The Program System TURBOMOLE. *Chem. Phys. Lett. 162*, 165–169.
34. Imhof, P., Noé, F., Fischer, S., and Smith, J. C. (2006) AM1/d Parameters for Magnesium in Metalloenzymes. *J. Chem. Theory Comput. 2*, 1050–1056.
35. Lopez, X., and York, D. M. (2003) Parameterization of semiempirical methods to treat nucleophilic attacks to biological phosphates: AM1/d parameters for phosphorous. *Theor. Chim. Acta 109*, 149–159.
36. Nam, K., Cui, Q., Gao, J., and York, D. M. (2007) Specific Reaction Parametrization of the AM1/d Hamiltonian for Phosphoryl Transfer Reactions: H, O, and P Atoms. *J. Chem. Theory Comput. 3*, 486–504.
37. Thiel, W. (2004) MNDO , version 6.1, Max-Planck-Institut fuer Kohlenforschung, Mülheim a.d. Ruhr, Germany.

38. Fischer, S., and Karplus, M. (1992) Conjugate Peak Refinement: An algorithm for finding reaction paths and accurate transition states in systems with many degrees of freedom. *Chem. Phys. Lett. 194*, 252–261.
39. Brooks, B. R., Bruccoleri, R. E., Olafson, B. D., States, D. J., Swaminathan, S., and Karplus, M. (1983) CHARMM: A program for macromolecular energy, minimization and dynamics calculations. *J. Comput. Chem. 4*, 187–217.
40. Klamt, A., and Schüürmann, G. (1993) COSMO: A New Approach to Dielectric Screening in Solvents with Explicit Expressions for the Screening energy and its Gradient. *J. Chem. Soc., Perkin Trans. 2*, 799–805.
41. Nosé, S. (1984) A unified formulation of the constant temperature molecular dynamics methods. *J. Chem. Phys. 81*, 511–519.
42. Hoover, W. G. (1985) Canonical dynamics: Equilibrium phase-space distributions. *Phys. Rev. A 31*, 1695–1697.
43. Ryckaert, J.-P., Ciccotti, G., and Berendsen, H. J. C. (1977) Numerical integration of the cartesian equations of motion of a system with constraints: Molecular dynamics of n-alkanes. *J. Comput. Phys. 23*, 327–341.
44. (a) Waszkowycz, B., Hillier, I. H., Gensmantel, N., and Payling, D. W. (1991) A combined quantum mechanical/molecular mechanical model of the potential energy surface of ester hydrolysis by the enzyme phospholipase A_2. *J. Chem. Soc., Perkin Trans. 2 2*, 225–231. (b) Waszkowycz, B., Hillier, I. H., Gensmantel, N., and Payling, D. W. (1991) A combined quantum mechanical/molecular mechanical model of inhibition of the enzyme phospholipase A_2. *J. Chem. Soc., Perkin Trans. 2 11*, 1819–1832. (c) Waszkowycz, B., Hillier, I. H., Gensmantel, N., and Payling, D. W. (1991) Combined quantum mechanical/molecular mechanical study of the catalysis by the enzyme phospholipase A_2: An investigation of the potential energy surface for amide hydrolysis. *J. Chem. Soc., Perkin Trans. 2 12*, 2025–2032.
45. Schwarzl, S. M., Huang, D., Smith, J. C., and Fischer, S. (2005) Non-Uniform Charge Scaling (NUCS): A practical approximation of solvent electrostatic screening in proteins. *J. Comput. Chem. 26*, 1359.
46. Imhof, P., Fischer, S., Krämer, R., and Smith, J. C. (2005) Density Functional Theory Analysis of Dimethylphosphate Hydrolysis: Effect of solvation and nucleophile variation. *THEOCHEM 713*, 1–5.